Study on the optical and electrical properties of tetracyanoethylene doped bilayer graphene stack for transparent conducting electrodes

Tej B. Limbu' , Frank Mendoza, Danilo Barrionuevo, Jennifer Carpena, Benji Maruyama, Ram S. Katiyar, Brad R. Weiner, and Gerardo Morell

Study on the optical and electrical properties of tetracyanoethylene doped bilayer graphene stack for transparent conducting electrodes

Tej B. Limbu,[1,2,a] Frank Mendoza,[1] Danilo Barrionuevo,[1,2]
Jennifer Carpena,[3,4] Benji Maruyama,[4] Ram S. Katiyar,[1,2] Brad R. Weiner,[1,5]
and Gerardo Morell[1,2]

[1]*Institute for Functional Nanomaterials, University of Puerto Rico, San Juan,
Puerto Rico 00931, United States*
[2]*Department of Physics, University of Puerto Rico, Rio Piedras Campus, San Juan,
Puerto Rico 00931, United States*
[3]*National Research Council, Washington D.C. 20001, United States*
[4]*Materials and Manufacturing Directorate, Air Force Research Laboratory, Wright-Patterson
Air Force Base, Dayton, Ohio 45433, United States*
[5]*Department of Chemistry, University of Puerto Rico, Rio Piedras Campus, San Juan,
Puerto Rico 00931, United States*

We report the optical and electrical properties of chemically-doped bilayer graphene stack by tetracyanoethylene, a strong electron acceptor. The Tetracyanoethylene doping on the bilayer graphene via charge transfer was confirmed by Raman spectroscopy and Infrared Fourier transform spectroscopy. Doped graphene shows a significant increase in the sheet carrier concentration of up to 1.520×10^{13} cm^{-2} with a concomitant reduction of the sheet resistance down to 414.1 Ω/sq. The high optical transmittance (*ca.* 84%) in the visible region in combination with the low sheet resistance of the Tetracyanoethylene-doped bilayer graphene stack opens up the possibility of making transparent conducting electrodes for practical applications. © *2016 Author(s). All article content, except where otherwise noted, is licensed under a Creative Commons Attribution (CC BY) license (http://creativecommons.org/licenses/by/4.0/).* [http://dx.doi.org/10.1063/1.4945345]

INTRODUCTION

The extraordinary properties of graphene, i.e. high electron mobility, high thermal and electrical conductivity, high optical transmittance, and high mechanical strength, make it a candidate material for numerous applications, including transparent conducting electrodes (TCEs).[1–4] In addition, its mechanical flexibility opens up the possibility to make bendable devices. The commercially available TCEs, such as Indium Tin Oxide (ITO) and Fluorine-doped Tin Oxide (FTO) will need substitutes in the near future due to the increasing cost of indium, intensive processing requirements, and the brittle nature of these metal oxides.[5–10] Graphene is studied as a potential mass-producible large-area TCE material because of its low sheet resistance (down to 64.2 Ω/sq) and a high optical transparency of 97.7% in the visible region.[11] These values correspond to the charge carrier concentration $\sim 10^{12}$ cm^{-2} and carrier mobility of 10^5 cm^{2}V^{-1}s^{-1}.[11] From the low sheet resistance and high optical transparency, graphene acquires a larger figure of merit ~ 250 than that of ITO (figure of merit ~ 223), which has a sheet resistance of 10 Ω/sq with 85% optical transparency in the visible region.[6] In other words, these properties of graphene make it a better TCE than ITO. Driven by these properties, there are many efforts to fabricate graphene-based TCEs. Recently, polycrystalline graphene, synthesized by chemical vapor deposition, has been shown to

---

[a]Author to whom correspondence should be addressed. Electronic mail: tejnembang@yahoo.com

have low sheet resistance of 125 Ω/sq with 97.4% optical transparency in the visible region.[12] However, these values still do not reach the standard set by ITO.

Chemical vapor deposition has been extensively employed to produce graphene films for device applications, but this technique yields polycrystalline graphene with significant levels of defects.[13–15] Grain boundaries and defects in graphene greatly affect its sheet resistance.[13,16–19] Grain boundary effects on the electrical properties can be avoided if single crystal graphene is grown. Some efforts have been made to directly synthesize single crystal large area graphene films on copper[20–23] and germanium substrates.[18] However, the sheet resistance is still relatively high due to defects, resist residues, and substrate effects.[24] These results show that the sheet resistance of graphene can vary by several orders of magnitude from 10^2 Ω/sq[12] through 10^4 Ω/sq,[25] which represent a big challenge for the commercial application of graphene as a transparent conducting electrode.

Two approaches have been shown to be effective in reproducibly reducing the sheet resistance: (1) doping and (2) stacking of graphene layers by multiple transfers on a transparent substrate. In this work, we present the optical and electrical properties of bilayer graphene stacks doped with tetracyanoethylene (TCNE) molecules in between the bilayer graphene sheets.

EXPERIMENTAL SECTION

Large area bilayer graphene was synthesized on 25 μm thick copper foil (Alfa Aesar, 99.8%) by a hot filament chemical vapor deposition (HFCVD) system (Blue Wave) using methane as a precursor gas. The concentration ratio by volume of methane and the hydrogen carrier gas was maintained at 1:5 during the deposition with a filament temperature of 2100 ^{0}C and substrate temperature of 850 ^{0}C keeping the pressure at 35 Torr. Following five minutes of deposition, the graphene-coated substrate was allowed to cool at the same pressure with the filaments and substrate heater turned off. More details of the synthesis method are available elsewhere.[19]

We transferred bilayer graphene onto pyrex or calcium fluoride substrates by the standard poly(methyl methacrylate) (PMMA) assisted wet-transfer method. A thin layer (ca. 1 μm) of PMMA (PMMA, MicroChem 950 A9) was deposited on top of the as-synthesized bilayer graphene on copper by spin coating followed by baking at 120 ^{o}C for 10 minutes. The copper was etched with 1 M ferric chloride (FeCl$_3$.6H$_2$O, Sigma Aldrich, 98%) solution. The resulting PMMA/graphene film was floated on a 10% HCl solution for 10 minutes to remove the residual Cu and FeCl$_3$ particles. The PMMA/graphene was then rinsed several times with deionized water and transferred onto the UV cleaned pyrex substrates that was placed overnight on a hot plate at 45 ^{o}C. Finally, the PMMA was dissolved in hot acetone to obtain graphene on the substrate.

In order to dope the deposited graphene with TCNE molecules, a 0.01 M TCNE (98%, Sigma Aldrich) solution in benzene (CAS Number 71-43-2, Sigma-Aldrich) was prepared and heated to 60 ^{o}C. The 0.01 M concentration corresponds to the number of TCNE molecules required to obtain a monolayer on 1 cm^2 of graphene/pyrex with a volume of 5 μL. The graphene/pyrex was wetted with the TCNE solution and allowed to dry. The PMMA/graphene was placed over the graphene/pyrex immediately after the benzene evaporated. The bilayer was baked at 45 ^{o}C for 24 hours in order to let the TCNE molecules rearrange, by surface adsorption, in between the bilayer graphene sheets. This baking step also allowed better adhesion between the different bilayers to form. Following the same procedure, we prepared a stack of three bilayer graphene sheets using the 0.01M TCNE solution.

In order to measure the graphene thickness, we performed atomic force microscopy (AFM) of graphene transferred onto SiO$_2$/Si in tapping mode in a Nanoscope V (Vecco) equipped with a silicon nitride tip with back side coating (Ti/Au 45 nm). High resolution transmission electron microscopy (TEM) analysis of the bilayer graphene was made with an FEI Talos TEM operated with 120 KV. The optical transparency of undoped and doped graphene was studied on pyrex substrates using a UV-visible spectrophotometer (Lambda 20, Perkin Elmer) and electrical resistivity and Hall measurements were carried out on pyrex substrates employing the Van der Pauw four probe method and averaged for each type of sample. Raman spectroscopy was done on a scanning micro-Raman system (Thermo Scientific DXR) equipped with a 532 nm laser source, and Fourier

transform infrared spectroscopy was done in the mid infrared region using a calcium fluoride window (Edmund Optics) on an FTIR spectrometer (Thermo Scientific DXR).

RESULTS AND DISCUSSION

Figure 1(a) shows a tapping mode AFM image of bilayer graphene on SiO_2/Si, where numerous wrinkles and folds of the broken parts are clearly visible. The inset shows the height profile of the graphene film scanned along the white line shown in Figure 1(a). The value of the step height measured for the graphene film lying flat on the SiO_2/Si is around 1.03 nm, a typical value for bilayer graphene. Figure 1(b) is the high resolution transmission electron microscopy (HRTEM) image of bilayer graphene. The fast Fourier transform of the HRTEM image in the inset shows two sets of six fold reflection spots corresponding to the two graphene monolayers of the bilayer system rotated with respect to each other with a twist angle of 30°.

A typical Raman spectrum of bilayer graphene synthesized by HFCVD reactor taken with a 532 nm excitation laser on pyrex substrate is shown in Figure 2 (black color). We found that the intense G and 2D peaks appear at 1582 cm^{-1} and 2683 cm^{-1}, respectively. The graphene has a small D-band (not shown) indicating a small defect density. A low intensity G* band originating from the double resonance intervalley process involving one in-plane transverse optical (TO) phonon and one longitudinal acoustic (LA) phonon[26] appears at 2455 cm^{-1}. The D' band is visible at 1620 cm^{-1} as a shoulder on the G band indicating that the defects introduced by the grain boundaries are
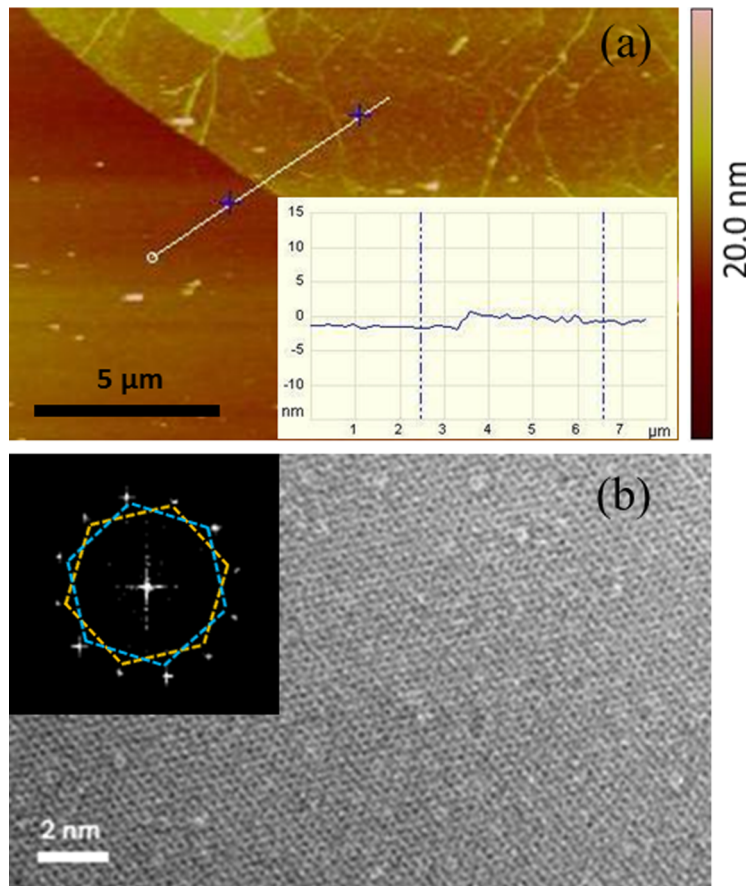

FIG. 1. (a) Representative tapping mode AFM image of bilayer graphene on SiO2/Si showing a folding region and wrinkles. Inset shows the height profile of the graphene film along the white line. (b) HRTEM image of the bilayer graphene. The FFT of the image in the inset shows that it is a twisted bilayer graphene with a twist angle of 30°.
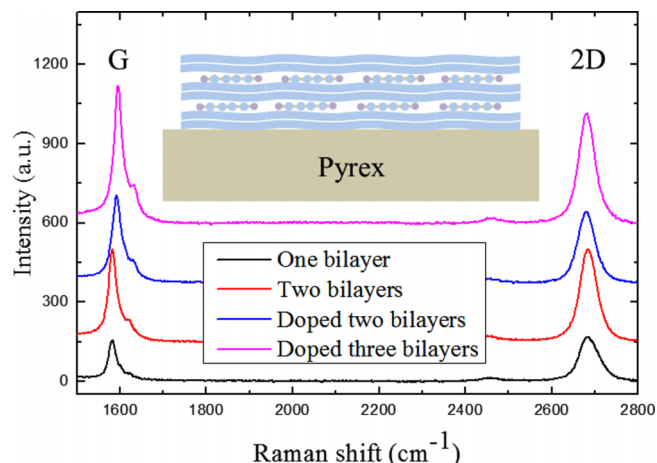
FIG. 2. Raman spectra of the graphene transferred onto pyrex showing the blue shifting of G peak and red shifting of 2D peak positions on charge transfer doping. A slight decrease in the intensity of 2D peak with respect to G peak is also visible. The inset is the schematic diagram of the TCNE-doped stack of three graphene bilayers. Each bilayer graphene is shown with a combination of two monolayers separated by a small space indicating van der Waals bonding.

significant in HFCVD graphene.[16] The shape of the 2D band is symmetric and can be fitted by a single Lorentzian, which is consistent with twisted bilayer graphene.[19,27]

The Raman spectrum of the doubly transferred bilayer graphene on pyrex is shown in red in Figure 2, which is similar to that of single transferred bilayer graphene except that the intensities of the Raman bands are roughly double in the doubly transferred bilayer graphene under the same experimental conditions. TCNE-doped double-transferred and triple-transferred bilayer graphene show some changes in the Raman spectra. TCNE is a strong electron acceptor molecule with a large electron affinity (EA = 3.17 eV) that readily forms charge-transfer complexes with host molecules or surfaces by pulling electrons from them.[28,29] When TCNE molecules are adsorbed on the graphene surface, electrons from graphene are transferred mainly to the nitrogen atoms of the cyano groups and to the central sp^2-bonded carbon atom.[28] Consequently, the graphene is p-doped (hole). The G band in the Raman spectrum is sensitive to this doping. In fact, the in-plane Raman G peak which is a doubly degenerate phonon mode at Γ point indicates the extent of the charge transfer. The G peaks in the TCNE-doped double-transferred and triple-transferred bilayer graphene are blue-shifted to 1590 cm^{-1} and 1592 cm^{-1} respectively due to phonon stiffening by charge extraction[30] consistent with the hole doping of graphene.[30–34] The 2D peak positions are found to be slightly red-shifted to 1581 cm^{-1} and 1580 cm^{-1}, respectively, similar to that observed by Chung et al.[34] for twisted bilayer graphene. In agreement with the previous reports, the 2D peak intensity decreases with respect to G peak intensity on the doped graphene as electron-electron scattering becomes competitive with electron-phonon scattering.[32,33] The overall Raman response of the twisted bilayer graphene is also dependent on the twist angle between the two monolayers and excitation laser energy.[34,35]

Fourier transform infrared spectroscopic (FTIR) studies were carried out to investigate the configuration of the tetracyanoethylene intercalated between the graphene layers (Figure 3). TCNE is a planar molecule with D_{2h} symmetry that can be detected by the IR absorption bands corresponding to its four cyano groups. We measured the FTIR spectrum of bare TCNE on a CaF2 window (Figure 3) for comparison purposes. The spectrum was obtained after the subtraction of the background spectrum due to CaF_2. Two bands, at 2227 cm^{-1} and 2262 cm^{-1}, were observed, corresponding to $C \equiv N$ stretch bands, in agreement with the previous reports.[36–39] The number of the bands and their positions may vary slightly depending upon the nature of the substrates and solvents used for the measurement.[37] The FTIR spectra for the stacks of doped two bilayers and three bilayers show two bands at 2220 cm^{-1} and 2237 cm^{-1}. The first band at 2220 cm^{-1} corresponds to the feature that appears at 2227 cm^{-1} in the spectrum of neat TCNE, i.e. it is red-shifted by 7 cm^{-1}. Figure 3(b) is the magnified portion of the spectra in Figure 3(a) in the region of the C≡N
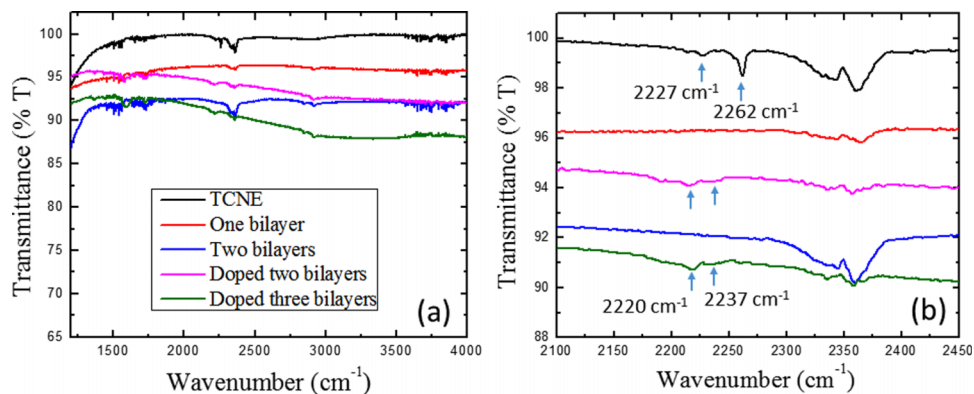
FIG. 3. (a) FTIR spectra of neat TCNE (black), one bilayer graphene (red), two bilayers (blue), two bilayers with TCNE intercalation between them (pink) and three bilayers with TCNE intercalation between them (green). (b) Magnified portion of the FTIR spectra in Figure 3(a) in the region of C≡N stretch bands.

stretch bands. Despite the fact that the number of intercalated TCNE molecules is low, the band can be clearly seen. This is consistent with an increase of the intensity of the nitrile stretch band due to the formation of charge transfer complexes with graphene.[40] As a comparison standard, we placed a relatively large amount of TCNE on a CaF2 window in order to obtain clear nitrile stretch bands at positions corresponding to the neat and crystalline substance. The red-shifting of the nitrile band takes place due to the weakening of the C≡N bond as it accepts electrons from graphene,[37,41] providing clear evidence of the charge transfer from graphene to the TCNE molecule. The band appearing at 2262 cm^{-1} for neat TCNE vanishes in the spectra for doped graphene and a new band appears at 2237 cm^{-1}. This may be attributed to the activation of the totally symmetric C≡N stretch mode by the formation of the charge transfer complex between TCNE and graphene, consistent with the results by Takenaka et al.[39] who observed the appearance of new IR bands in similar complexes with alkali halides. In addition to the above discussed IR bands, a new band at around 1584 cm^{-1} appears for doped bilayer graphene. This band is assigned to the totally symmetric C=C stretch mode which is typically IR forbidden and Raman active,[37] but becomes activated in the infrared spectrum by virtue of the electron affinity of the acceptor molecule (TCNE) in the planar sandwich complexes.[39] Other IR bands observed in all of the undoped and doped graphene are: (1) the bands at 2360 cm^{-1} corresponding to the asymmetric stretch mode of atmospheric carbon dioxide which is routinely observed in the background scan on an FTIR measurement; and (2) the low intensity bands appearing at around 2850 cm^{-1} and 2926 cm^{-1} corresponding to the symmetric and asymmetric stretch modes of C-H bonds, respectively, most likely due to traces of PMMA residues on the graphene surface or partial hydrogenation of the graphene.

The small redshift (~7 cm^{-1}) of the C≡N band in doped graphene corresponds to the small amount of charge transfer. The amount of charge transfer is linearly correlated with the nitrile band red-shifting.[36,41] Furthermore, the electron transfer from graphene to the TCNE molecule is also dependent upon the coverage of the TCNE molecule on the graphene surface. Lu et al.,[28] using density functional theory, calculated the charge transfer between TCNE and single layer graphene at two different coverages, 1.04% and 4.20% of TCNE on graphene. They found ~0.44e and 0.20e per TCNE molecule charge transfer from graphene to each TCNE molecule, respectively. In our case, the TCNE coverage on the graphene surface is higher than in the calculations of Lu et al. leading to an increased intermolecular repulsive interaction and reduced TCNE-graphene interaction. As a result, the charge transfer is also reduced. However, due to a large number of TCNE molecules per unit surface area of graphene, the overall charge transfer from graphene to the TCNE molecules becomes more efficient and the overall hole doping on graphene by charge transfer is maximized. A noteworthy point in the case of chemical doping of bilayer graphene is that due to the charge depletion in the graphene monolayer adsorbed with an interacting molecule (TCNE), the potential equivalence between two layers is broken and a band gap opens at the Dirac point, the magnitude of which depends upon the amount of charge depletion in the graphene.[28]
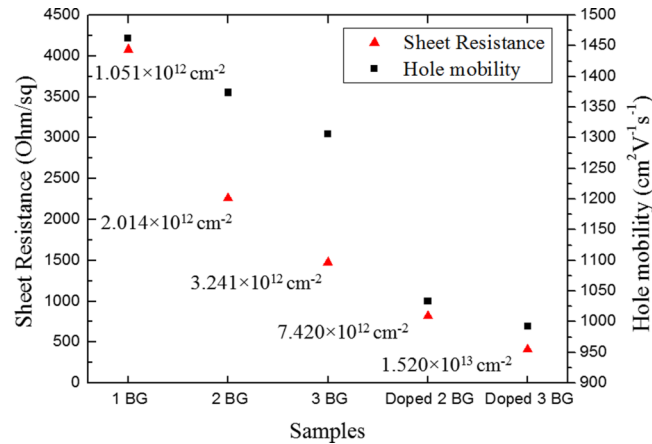
FIG. 4. Sheet resistance, charge carrier concentration and hole mobility values of the undoped and doped graphene. Note: BG stands for bilayer graphene.

Sheet resistance, hole mobility and sheet carrier concentration are presented in Figure 4. Hall effect studies on the TCNE-doped graphene showed that the charge carriers are p-type with a concentration of 1.520×10^{13} cm^{-2} for the doped stack of three bilayers, which is about 15 times the carrier concentration of 1.051×10^{12} cm^{-2} for a single bilayer. The carrier concentration of the undoped stack of two bilayers is 2.014×10^{12} cm^{-2}, while that of the doped stack of two bilayers is 7.420×10^{12} cm^{-2}, which is an intermediate value as expected. The sheet carrier concentration for undoped stack of three bilayers is 3.241×10^{12} cm^{-2}, which is less than half the value for the doped stack of two bilayers. The sheet resistance value decreases as we increase the number of graphene layers in the stack and dope with TCNE. Our bilayer graphene has a sheet resistance of about 4078 Ω/sq. The value is reduced to about half (2263 Ω/sq) for a stack of two bilayers, due to the introduction of two independent channels for electron flow. Sheet resistance of the undoped stack of three bilayers further decreases to 1477 Ω/sq. The TCNE intercalated stack with two bilayers shows a reduction of the sheet resistance value to 822.6 Ω/sq while the doped three bilayer stack has a sheet resistance of 414.1 Ω/sq. The hole mobility of our bilayer graphene is measured to be 1462 cm^{2}V^{-1}s^{-1} which decreases slightly to 1374 cm^{2}V^{-1}s^{-1} and 1306 cm^{2}V^{-1}s^{-1} corresponding to an undoped double and triple bilayer graphene respectively due to some level of interaction taking place at the contact points between the two adjacent bilayers. However, the hole mobility is found to be significantly smaller (1033 cm^{2}V^{-1}s^{-1}) in the case of the doped two bilayers which is attributed mainly to increased charge carrier scattering in the graphene by the perturbation from TCNE. Mobility for the doped three-layer stack is 993.2 cm^{2}V^{-1}s^{-1}, almost the same as in the doped two layer stack.

Sheet resistance (R_s) is inversely related to the sheet charge carrier concentration (n) and charge mobility (μ) as $R_s = 1/\mu en$ where, e is the electron charge. The charge carrier mobility is an intrinsic property of a material so it cannot be increased. It is possible to increase the sheet carrier concentration of the graphene stack via doping. The factor contributing to the low sheet resistance of the doped graphene stack is the increased sheet carrier concentration. The sheet hole carrier concentration is increased significantly in the case of a doped three-layer stack despite a small reduction in carrier mobility. Overall, the sheet resistance is reduced significantly in the doped three layered stack.

By increasing the number of the graphene layers in the stack, the sheet resistance decreases, but at the same time optical transparency is also degraded. Figure 5 shows the optical transmittance of the undoped and doped graphene from the near infrared to the visible region. The optical transmittance of our bilayer graphene at 550 nm is around 94.5%, while that of double and triple bilayer graphene are 90.0% and 85.5%, respectively. The optical transmittance of the doped double and triple bilayer graphene is not affected significantly, which we measured to be around 88.5% and 84.0%, respectively.
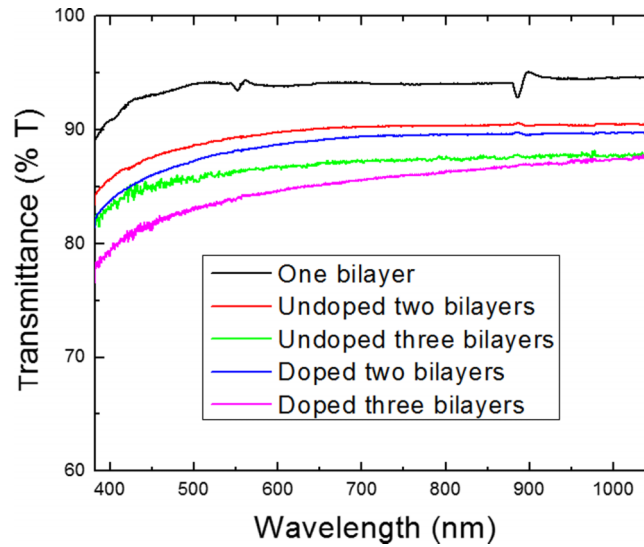
FIG. 5. Optical transmittance of single bilayer graphene (black), undoped stack of two bilayers (red), undoped stack of three bilayers (green), doped stack of two bilayers (blue), and doped stack of three bilayers (pink).

Optical transmittance of the graphene sheet is directly derived from its universal optical conductivity $\sigma(\omega)$ at frequency ω. It is solely determined by fundamental constants as $\sigma(\omega) = \pi e^2/2h$[42] where e is the electron charge and h is Planck's constant. Optical absorption is obtained from the conductivity as $A(\omega) = (4\pi/c)\,\sigma(\omega) = \pi\alpha \approx 2.29\%$ for a monolayer graphene, where c is the speed of light and α is the fine structure constant which equals $e^2/\hbar c$, $\hbar = h/2\pi$ being the reduced Plank's constant. Hence, considering negligible or no reflectance from graphene, optical transmittance is equal to $1 - A(\omega)$. The optical transmittance of bilayer graphene is slightly lower than the theoretical value 95.6%, which may be due to some level of inevitable contamination of the graphene obtained during transfer. TCNE has a strong absorption band in the range $250-270$ nm and on interaction with few layer graphene, shows a shallow and wide charge transfer band in $550-750$ nm region.[33] In our case, the charge transfer band is not visible most likely due to the shallow and wide nature of the spectral feature. A high optical transparency in the visible region is important as TCEs have to maximize the visible light that is passing through. In addition to the optical transmittance in the visible region, we also noted that the optical transmittance of our undoped and doped graphene stacks follows the relation, $T = (1 - N\pi\alpha)$ in the mid infrared region as measured by FTIR where N is the number of monolayers. Mid IR transmittance of the bilayer graphene measured on a CaF2 window is about 96.0% while that of two stacked bilayers is about 92.5% in the range 1000 to 4000 cm^{-1}, close to theoretical value $(1 - 2\pi\alpha)$ for bilayer graphene and $(1 - 4\pi\alpha)$ for a stack of two bilayers, derived from universal conductivity. Optical transmittance values for the doped stacks of two and three bilayers are increasing for certain wavenumbers. As it can be seen from the Figure 3(a), the transmittance values of the doped graphene stacks of two and three bilayers are 92.0% and 88.0%, respectively, above 3300 cm^{-1}, whereas the transmittance increases gradually from 3300 cm^{-1} until 2000 cm^{-1}. The increase in the optical transmittance can be ascribed to the suppression of the interband optical transition for photon energy $\omega < 2E_F$ by Pauli blocking[42,43] where EF is the Fermi energy in graphene. The TCNE interaction with graphene produces hole doping in graphene, which is characterized by the downshifting of the Fermi level in graphene below the Dirac point.

In the mid infrared region, the shift in the Fermi level E_F can be determined by using Pauli blocking interband transitions.[42] The threshold energy for the increased optical transmittance roughly gives the value of $2E_F$.[42] Taking the example of our doped stack of three bilayers, the value of the threshold energy $2E_F$ extracted from the FTIR spectrum is around 2650 cm^{-1}, so the value of EF should be around 1325 cm^{-1} (0.164 eV). On the other hand, the charge carrier concentration obtained by Hall measurements in the doped stack of three bilayers is 1.520×10^{13} cm^{-2}. Assuming

that the doping on all the graphene monolayers is the same, the charge carrier concentration per monolayer is calculated to be 2.541×10^{12} cm^{-2} from which the Fermi energy can be calculated by the relation $E_F = \hbar v_f \sqrt{n\pi}$ where, v_f (=10^8 cm/s) is the Fermi velocity in graphene. The value of E$_F$ so obtained is 0.185 eV, which is in reasonable agreement to the value of E$_F$ extracted from the FTIR spectra. Furthermore, the shift in the Fermi level in doped graphene stack can be related roughly to the G peak position shift in the Raman spectra (Figure 2). For a p-doped monolayer graphene, the G peak position is given by the relation, $45 \times |E_F| = \omega_G - 1583.8 \ eV$.[34] Taking the G peak position ~1592 cm^{-1} for the doped stack of three bilayers, we obtain E$_F$ equal to 0.182 eV, consistent with the E$_F$ values obtained directly from the carrier concentration and FTIR transmittance spectra.

The TCNE doped stack of three bilayer graphene results in a sheet resistance of 414.1 Ω/sq at an optical transparency of 84.0% in the visible region. These physical properties remain stable for at least 5 months. Hence, although TCNE is toxic, it appears to remain trapped in the device. These results are still below the minimum industry standard for ITO replacement materials, where a sheet resistance of R$_S$ < 100 Ω/sq coupled with transmittance of T > 90% in the visible region is required;[6] nonetheless, they reached the requirements for touch screen (500 Ω/sq, 85%) applications.[44] As a TCE, TCNE-doped graphene is comparable to several previously reported results,[5–9,44–48] which are below or close to the requirements for practical TCEs set by ITO. However, the properties of TCNE-doped graphene are still below those reported in references 12, 30, 31, 43, and 49–51, which are above the TCE requirements. The values of both sheet resistance and optical transmittance of the TCEs in these reports are rather scattered which imposes a

TABLE I. Values of sheet resistance, optical transparency and corresponding Figure of Merit (FoM) of the TCEs reported in the references cited above.

References	Materials and Fabrication method	Sheet Resistance (Ω/sq)	Transmittance (%)	FoM
46	Graphene Oxide ink coating on glass plate by Meyer rod method	5000	40	0.07
48	Spin coated graphene oxide followed by reduction	5000	80	0.32
8	Thermally reduced graphene oxide	1818.18	70	0.53
5	CVD grown graphene on Nickel substrate	230	72	4.59
This work	TCNE-doped HFCVD grown bilayer graphene stack	414.1	84	5.00
47	Large-scale graphene films grown by chemical vapor deposition on thin nickel layers	280	80	5.70
45	Multiple transfers of CVD grown monolayer graphene	350	90	9.96
9	Multiple transfers of low pressure CVD grown bilayer graphene stack	180	83	10.73
7	Nitric acid doped monolayer graphene stack	90	80	17.74
44	Nitric acid treated film of carbon nanotubes prepared by spray method	40	70	24.14
6	Minimum industry standard	<100	>90	34.85
30	AuCl$_3$ doped monolayer graphene stack	54	85	41.24
49	Copper nanowire-graphene core-shell nanostructure	51.8	90.8	73.61
12	Nitric acid doped stack of four CVD grown graphene monolayers	30	90	116.16
50	Integration of CVD grown monolayer graphene with Silver nanowires	24	91	162.66
31	Ferric Chloride doped few layer graphene obtained by micromechanical cleavage of graphite	8.8	84	235.16
51	Roll-to-Roll encapsulation of Silver nanowires between monolayer graphene and plastic Substrate	8	94	749.89
43	Lithium intercalated exfoliated ultrathin graphite	3	91.7	1400.00

difficulty in the direct comparison of the devices for their opto-electrical performance. The direct comparison among the TCEs fabricated in the references can be made by using the relation, $T = \left(1 + \frac{Z_0}{2R_S} \cdot \frac{1}{FoM}\right)^{-2}$, where Z_0 is the impedance of free space and has the value 377 Ω, R_S is the sheet resistance and T is the optical transmittance. The FoM (Figure of Merit) $= \sigma_{DC}/\sigma_{OP}$ is a parameter which indicates the performance of TCEs where σ_{DC} and σ_{OP} are the three dimensional DC conductivity and optical conductivity respectively. For better opto-electrical properties i.e. high T and low R_s, a higher value of FoM is obtained. We calculated the FoM values of the TCEs reported in the above references for comparison. The values of the sheet resistance, optical transmittance and the resulting FoM are shown in Table I. Note that for more stringent conditions, the sheet resistance and optical transparency values necessary are $R_S < 10$ Ω/sq and $T > 85\%$ with a FoM > 223.[6] This condition is met by only a few of the TCEs presented in Table I. Another noteworthy point is that the TCEs presented in Table I have been chosen based on their opto-electrical performance. The straightforward comparison of the TCEs based on FoM values does not give the whole picture since good TCEs are characterized by other qualities, such as their chemical inertness, stability, mechanical flexibility, strain resistance, low cost of fabrication, environmentally friendliness, and suitability for integration with practical devices.

CONCLUSIONS

We studied the optical and electrical properties of TCNE-doped bilayer graphene stacks. Layer by layer transfer of a relatively small number of HFCVD-grown large area and uniform bilayer graphene sheets onto transparent substrates minimizes the risk of graphene breakdown while saving time and cost. The results show the occurrence of charge transfer doping of the bilayer graphene stack by TCNE, which produces a 15-fold increase in the charge carrier concentration for 6.4 µg/cm^2 of TCNE on graphene, thereby reducing the sheet resistance of the graphene stack while maintaining high optical transparency. The encouraging properties observed for the electrical and optical characteristics with a modest surface density of TCNE on graphene indicate that this system could be explored further. The simple fabrication and transfer methods are attractive and useful for rapid analysis of the properties of bilayer graphene.

ACKNOWLEDGEMENTS

[1] Zainab Zafar, Zhen Hua Ni, Xing Wu, Zhi Xiang Shi, Hai Yan Nan, Jing Bai, and Li Tao Sun, CARBON **61**, 57–62 (2013).

[2] A.K. Geim and K.S. Novoselov, Nat. Mater. **6**, 183–191 (2007).

[3] A.K. Geim, Science **324**, 1530–1534 (2009).

[4] Arun Kumar Singh, Muneer Ahmad, Vivek Kumar Singh, Koo Shin, Yongho Seo, and Jonghwa Eom, ACS Appl. Mater. Interfaces **5**, 5276–5281 (2013).

[5] Lewis Gomez De Arco, Yi Zhang, Cody W. Schlenker, Koungmin Ryu, Mark E. Thompson, and Chongwu Zhou, ACS Nano **4**(5), 2865–2873 (2010).

[6] Sukanta De and Jonathan N. Coleman, ACS Nano **4**(5), 2713–2720 (2010).

[7] Amal Kasry, Marcelo A. Kuroda, Glenn J. Martyna, George S. Tulevski, and Ageeth A. Bol, ACS Nano **4**(7), 3839–3844 (2010).

[8] Xuan Wang, Linjie Zhi, and Klaus Müllen, Nano Lett. **8**, 1 (2008).

[9] Seunghyun Lee, Kyunghoon Lee, Chang-Hua Liu, and Zhaohui Zhong, arXiv:1112.1378 [cond- mat.mes-hall].

[10] Ryousuke Ishikawa, Masashi Bando, Yoshitaka Morimoto, and Adarsh Sandhu, Nanoscale Research Letters **6**, 111 (2011).

[11] Shuping Pang, Yenny Hernandez, Xinliang Feng, and Klaus Müllen, Adv. Funct. Mater. **23**, 2779–2795 (2011).

[12] Sukang Bae, Hyeongkeun Kim, Youngbin Lee, Xiangfan Xu, Jae-Sung Park, Yi Zheng, Jayakumar Balakrishnan, Tian Lei, Hye Ri Kim, Young Il Song, Young-Jin Kim, Kwang S. Kim, Barbaros Özyilmaz, Jong-Hyun Ahn, Byung Hee Hong, and Sumio Iijima, Nat. Nanotech **5**, 574–578 (2010).

[13] Zhuhua Zhang, Yang Yang, Fangbo Xu, Luqing Wang, and Boris I. Yakobson, Adv. Funct. Mater **25**, 367–373 (2015).

[14] K. Kim, Z. Lee, W. Regan, C. Kisielowski, M. Crommie, and A. Zettl, ACS Nano **5**, 2142 (2011).

[15] P. Y. Huang, C. S. Ruiz-Vargas, A. M. van der Zande, W. S. Whitney, M. P. Levendorf, J. W. Kevek, S. Garg, J. S. Alden, C. J. Hustedt, and Y. Zhu, Nature **469**, 389 (2011).

[16] Axel Eckmann, Alexandre Felten, Artem Mishchenko, Liam Britnell, Ralph Krupke, Kostya S. Novoselov, and Cinzia Casiraghi, Nano Lett. **12**(8), 3925–3930 (2012).

[17] Alex W. Robertson, Christopher S. Allen, Yimin A. Wu, Kuang He, Jaco Olivier, Jan Neethling, Angus I. Kirkland, and Warner, Nature Communications **3**, 1144 (2012).

[18] Jae-Hyun Lee, Eun Kyung Lee, Won-Jae Joo, Yamujin Jang, Byung-Sung Kim, Jae Young Lim, Soon-Hyung Choi, Sung Joon Ahn, Joung Real Ahn, Min-Ho Park, Cheol-Woong Yang, Byoung Lyong Choi, Sung-Woo Hwang, and Dongmok Whang, Science **18**, 344 (2014).

[19] Frank Mendoza, Tej B. Limbu, Brad R. Weiner, and Gerardo Morell, Diamond and Relat. Mat. **51**, 34–38 (2015).

[20] Xuesong Li, Carl W. Magnuson, Archana Venugopal, Rudolf M. Tromp, James B. Hannon, Eric M. Vogel, Luigi Colombo, and Rodney S. Ruoff, J. Am. Chem. Soc. **133**(9), 2816–2819 (2011).

[21] Zheng Yan, Jian Lin, Zhiwei Peng, Zhengzong Sun, Yu Zhu, Lei Li, Changsheng Xiang, E. Loïc Samuel, Carter Kittrell, and James M. Tour, ACS Nano **6**(10), 9110–9117 (2012).

[22] Hong Wang, Guanzhong Wang, Pengfei Bao, Shaolin Yang, Wei Zhu, Xing Xie, and Wen-Jun Zhang, J. Am. Chem. Soc. **134**, 3627–3630 (2012).

[23] Chaocheng Wang, Wei Chen, Cheng Han, Guang Wang, Binbing Tang, Changxin Tang, Yan Wang, Wennan Zou, Wei Chen, Xue-Ao Zhang, Shiqiao Qin, Shengli Chang, and Li Wang, SCIENTIFIC REPORTS **4**(2014), 4537 (2014).

[24] Chun Ning Lau, Wenzhong Bao, and Jairo Velasco, Jr., Materialstoday **15**(6), 238–245 (2012).

[25] L. Hao, J. Gallop, S. Goniszewski, O. Shaforost, N. Klein, and R. Yakimova, Appl. Phys. Lett. 123103 (2013).

[26] L.M. Malard, M.A. Pimenta, G. Dresselhaus, and M.S. Dresselhaus, Physics Reports **473**, 51–87 (2009).

[27] Daniel R. Lenski and Michael S. Fuhrer, J. Appl. Phys. **110**, 013720 (2011).

[28] Y. H. Lu, W. Chen, Y. P. Feng, and P. M. He, J. Phys. Chem. B **113**(1), (2009).

[29] Daniel Wegner, Ryan Yamachika, Yayu Wang, Victor W. Brar, Bart M. Bartlett, Jeffrey R. Long, and Michael F. Crommie, Nano Lett. **8**(1), 131— 135 (2008).

[30] Fethullah Günes, Hyeon-Jin Shin, Chandan Biswas, Gang Hee Han, Eun Sung Kim, Seung Jin Chae, Jae-Young Choi, and Young Hee Lee, ACS Nano **4**(8), 4595–4600 (2010).

[31] Ivan Khrapach, Freddie Withers, Thomas H. Bointon, Dmitry K. Polyushkin, William L. Barnes, Saverio Russo, and Monica F. Craciun, Adv. Mater **24**, 2844–2849 (2012).

[32] Andrew C. Crowther, Amanda Ghassaei, Naeyoung Jung, and Louis E. Brus, ACS Nano **6**(2), 1865–1875 (2012).

[33] Rakesh Voggu, Barun Das, Chandra Sekhar Rout, and C N R Rao, J. Phys.: Condens. Matter **20**, 472204 (2008).

[34] Ting-Fung Chung, Rui He, Tai-Lung Wu, and Yong P. Chen, Nano Lett. **15**(2), 1203–1210 (2015).

[35] Kwanpyo Kim, Sinisa Coh, Liang Z. Tan, William Regan, Jong Min Yuk, Eric Chatterjee, M. F. Crommie, Marvin L. Cohen, Steven G. Louie, and A. Zettl, PRL **108**, 246103 (2012).

[36] A. Pawlukojć, W. Sawka-Dobrowolska, G. Bator, L. Sobczyk, E. Grech, and J. Nowicka-Scheibe, Chemical Physics **327**, 311–318 (2006).

[37] Joel S. Miller, Angew. Chem. Int. Ed. **45**, 2508–2525 (2006).

[38] Siham Y. AlQaradawi and El-Metwally Nour, Spectrochimica Acta Part A **62**, 578–581 (2005).

[39] Tohru Takenaka, Shin-ichi Tadokoro, and Natsu Uyeda, Bull. Inst. Chem. Res. **48**(6), 249–263 (1970).

[40] Seema Bagchi (Chattaraj), Kakali Sharma, Ashutosh Chakrabortty, and Sujit Chandra Lahiri, Spectrochimica Acta Part A: Molecular and Biomolecular Spectroscopy **95**, 637–647 (2012).

[41] Diana Nanova, Sebastian Beck, Andreas Fuchs, Tobias Glaser, Christian Lennartz, Wolfgang Kowalsky, Annemarie Pucci, and Michael Kroeger, Organic Electronics **13**, 1237–1244 (2012).

[42] Kin Fai Mak, Long Ju, Feng Wang, and Tony F. Heinz, Solid State Communications **152**, 1341–1349 (2012).

[43] Wenzhong Bao, Jiayu Wan, Xiaogang Han, Xinghan Cai, Hongli Zhu, Dohun Kim, Dakang Ma, Yunlu Xu, Jeremy N. Munday, H. Dennis Drew, Michael S. Fuhrer, and Liangbing Hu, Nature Communications **5**, 4224 (2014).

[44] Hong-Zhang Geng, Ki Kang Kim, Kang Pyo So, Young Sil Lee, Youngkyu Chang, and Young Hee Lee, J. AM. CHEM. SOC. **129**, 7758–7759 (2007).

[45] Xuesong Li, Yanwu Zhu, Weiwei Cai, Mark Borysiak, Boyang Han, David Chen, Richard D. Piner, Luigi Colombo, and Rodney S. Ruoff, Nano Lett. **9**, 4359–4363 (2009).

[46] Jingjing Wang, Zhiqiang Fang, Hongli Zhu, Binyu Gao, Sean Garner, Pat Cimo, Zachary Barcikowski, Alice Mignerey, and Liangbing Hu, Thin Solid Films **556**, 13–17 (2014).

[47] Keun Soo Kim, Yue Zhao, Houk Jang, Sang Yoon Lee, Jong Min Kim, Kwang S. Kim, Jong- Hyun Ahn, Philip Kim, Jae-Young Choi, and Byung Hee Hong, Nature **457**, 706–710 (2009).

[48] Junbo Wu, Héctor A. Becerril, Zhenan Bao, Zunfeng Liu, Yongsheng Chen, and Peter Peumans, Appl. Phys. Lett. **92**, 263302 (2008).

[49] Yumi Ahn, Youngjun Jeong, Donghwa Lee, and Youngu Lee, ACS NANO **9**(3), 3125–3133 (2015).

[50] Iskandar N. Kholmanov, Carl W. Magnuson, Ali E. Aliev, Huifeng Li, Bin Zhang, Ji Won Suk, Li Li Zhang, Eric Peng, S. Hossein Mousavi, Alexander B. Khanikaev, Richard Piner, Gennady Shvets, and Rodney S. Ruoff, Nano Lett. **12**, 5679–5683 (2012).

[51] Bing Deng, Po-Chun Hsu, Guanchu Chen, B. N. Chandrashekar, Lei Liao, Zhawulie Ayitimuda, Jinxiong Wu, Yunfan Guo, Li Lin, Yu Zhou, Mahaya Aisijiang, Qin Xie, Yi Cui, Zhongfan Liu, and Hailin Peng, Nano Lett. **15**, 4206–4213 (2015).